JOURNAL OF GUIDANCE, CONTROL, AND DYNAMICS
Vol. 33, No. 6, November–December 2010

Engineering Notes

Transfers to Sticky Distant Retrograde Orbits

Christopher J Scott* and David B. Spencer†
Pennsylvania State University,
University Park, Pennsylvania 16802

DOI: 10.2514/1.47792

Introduction

THIS work explores transfers to sticky distant retrograde orbits in the sun–Earth system, extending the methodologies of [1]. These orbits are of value to spacecraft that have little or no propulsive means and must rely on the natural dynamics of the system.

Sticky regions retain orbits characterized by a dynamical lifetime longer than predicted by the Lyapunov time [2]. A sizeable stable region encompasses the central stable periodic distant retrograde orbits (SPDRO), family f [3], at nearly all energies. Its frontier is marked by a homoclinic tangle originating from a period-3 unstable periodic orbit known as a bounding unstable periodic orbit (BUPO) classified as family g^3 [3]. The manifolds form lobes which dictate transport into and out of the sticky region. Objects exhibiting the largest capture times are shown to be responsible for extended capture.

As sets of collisions exist across energy surfaces piercing the sun–Earth line perpendicularly [1], there exist analogous structures without this constraint. A differential-correction algorithm was developed that modifies the terminal radial velocity for transfers following these sets. Developments facilitate the preliminary design of two transfers. The first uses a single maneuver before coasting into the fringe of the stable region followed by a lengthy capture. Such natural trajectories can be used by spacecraft with no propulsion, such as the one proposed in the Regatta-Astro program of the former Soviet Union [4]. The second transfer involves two impulsive maneuvers. The first starts from low Earth orbit before entering into an orbit of extended capture. After a coasting phase, a small impulsive stabilizing maneuver is performed to insert into a stable quasi-periodic distant retrograde orbit (QPDRO). The transfer can result in significant fuel savings compared to direct insertion into the SPDRO.

Algorithm and Phase Space

The circular restricted three body problem (CR3BP) is used, where a "massless" particle evolves under the influence of two massive bodies revolving in circular orbits about their barycenter. With its x axis pointing toward the larger primary the coordinate system rotates at constant angular velocity with respect to the inertial coordinate system. Under these assumptions there exists a constant of motion, known as the Jacobi constant C [5]. As in [1,6], an augmented Earth-plus-moon model is adopted. This approximation entails combining the Earth and moon into the second primary. In addition, the radius of the parking orbit is increased, so that the velocity is that of a circular orbit at a specific altitude. A realistic multibody simulation proved that this modification provides accurate results [6]. A mass ratio of 3.04042×10^{-6} and an absolute tolerance of 1×10^{-10} were used for all simulations. All plots have their origins shifted to Earth.

This study uses an algorithm similar to the one first introduced in [1], yet modifies the radial velocity. The nomenclature of the F1–F5 transfer families is also introduced in [1]. F1 and F2 correspond to Ocampo's class A and B transfers [6] for a range of larger SPDROs. Figure 1 displays multiple F1 and F2 transfers terminating on the x axis at $C = -1.4990$.

The arrangement of collision sets at $Vx = 0$, indicates that analogous regions exist for arbitrary values. Figure 2a verifies this assumption on a backward collision map on a surface of section (SOS) at $y = 0$, $\dot{y} < 0$.

F1–F5 follow sets that cross $Vx = 0$, yet many do not cross this hyperplane suggesting the existence of additional families. Using the methodologies of [1] it is possible to follow the boundaries of the collision sets in the same manner that transfer families are continued through energy. Figure 2b reveals the complicated structure of phase space showing multiple crossings of each family with the collision sets.

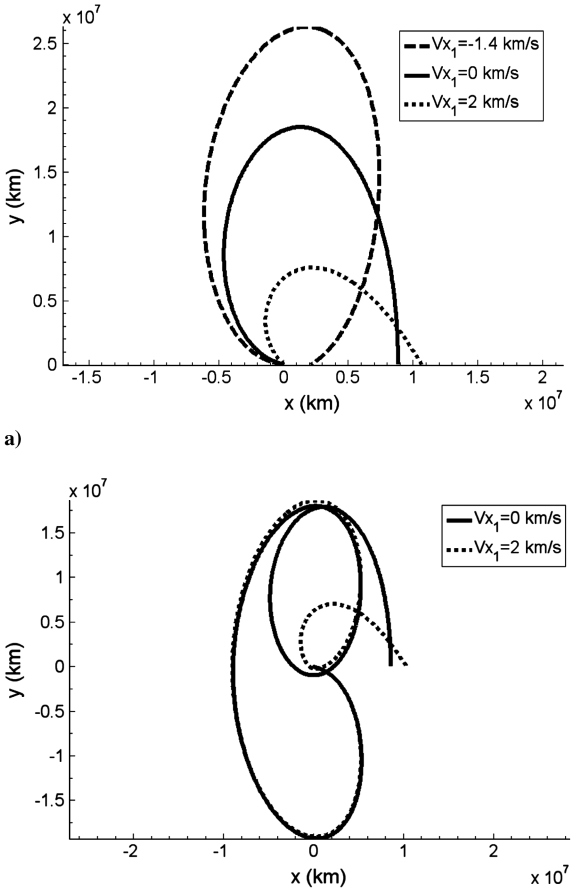

Fig. 1 Plots of a) F1 and b) F2 transfers terminating with indicated Vx at $C = -1.4990$.

Received 23 October 2009; revision received 15 July 2010; accepted for publication 18 July 2010.

*Graduate Student, Department of Aerospace Engineering, 229 Hammond Building. Student Member AIAA.

†Associate Professor, Department of Aerospace Engineering, 229 Hammond Building. Associate Fellow AIAA.

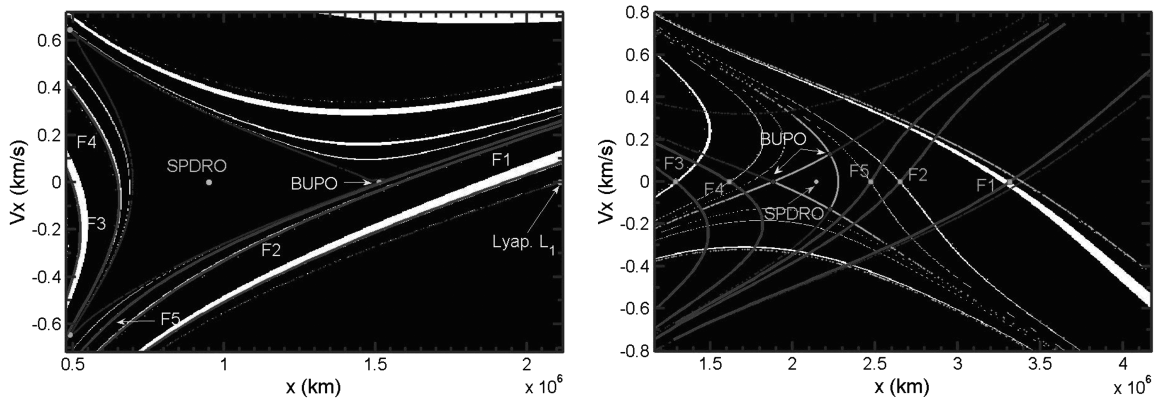

a) b)

Fig. 2 Collision maps: a) backward at $C = -1.5001$ over a period of two years and the termination points of the F1–F5 transfer families with variable Vx and b) forward at $C = -1.4999$ over a period of two years including the manifolds of the BUPO and L_1 Lyapunov orbit and continuations of the F1–F5 transfers through Vx with no second burn. Black and white indicate no collision and collision, respectively.

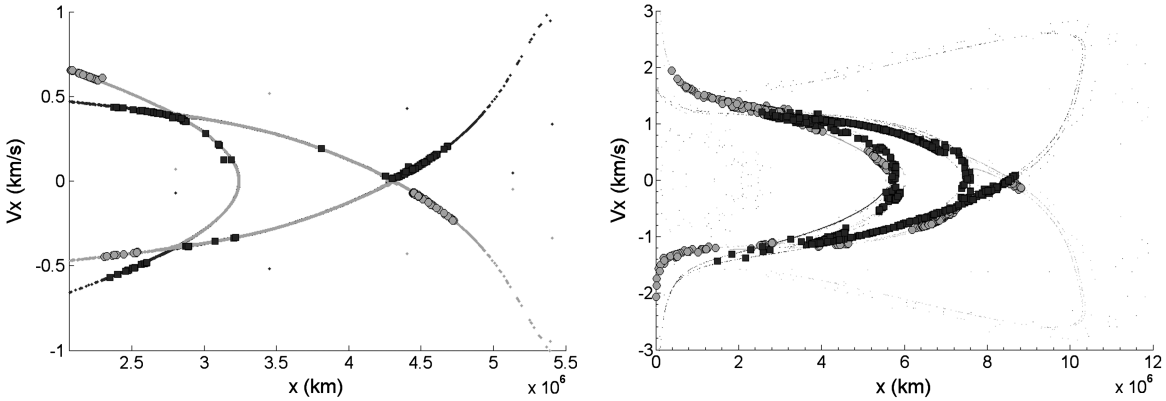

a) b)

Fig. 3 First and last intersections, shown as circles and squares, of surviving members of 5×10^5 particles over 10-year simulations. Stable and unstable manifolds of the BUPO are shown: a) at $C = -1.4997$ simulation terminates upon collision or escape beyond a distance of 20 times the radius of the Hill sphere with 183 survivors, 8524 collisions, and 491,293 escapes and b) at $C = -1.4990$ simulation terminates after collision or until particle reaches 30 times the radius of the Hill sphere with 939 survivors, 5508 collisions, and 493,553 escapes.

Capture Dynamics

Two types of temporary capture are presented. The first evolves within the lobes of the stable manifold. These orbits are characterized by modest to drastic increases in capture times compared to nearby orbits. The second are capture orbits outside of the lobes. These have a fleeting presence in the region excluding those that lie close to the BUPO at a low stability index.

To demonstrate the mechanisms of capture a simple numerical experiment can be performed. At a given energy, orbits are propagated from initial conditions uniformly sampled on a circle in physical space whose radius is a multiple of the radius of the Hill sphere. The velocity is sampled at a specified energy with a randomly chosen direction. Care is taken to ensure the circle does not intersect the stable region. The simulation continues until the particle collides with the planet, escapes from the planetary region, or survives after some maximum time. For those that survive, the avenues of capture, escape, and regions of extended capture are revealed by recording the first and last intersections with the SOS. In dynamical astronomy a similar procedure has been used to attain capture statistics [7–9].

The first intersections of orbits surviving a simulation of 10 years lie inside or near lobes of the stable manifold, shown in Fig. 3. The squares mark the last intersection of surviving orbits trapped near or within the homoclinic tangle. The number of survivors outside of the lobes goes to zero as simulation time is increased. There are many more surviving particles at $C = -1.4990$, because of the relatively large width of the lobes intersecting the Hill sphere. They are cycled through the lobe dynamics which delays divergence from the region [10].

Using the linearized dynamics near the BUPO, an estimate of the rate of divergence can be obtained using the stability index, k. Figure 4 shows the evolution of the stability index with energy. A large value indicates a high rate of divergence.

Values continue to increase for $C < -1.5001$ and $C > -1.4997$. The stability threshold corresponds to the crossing of the BUPO and

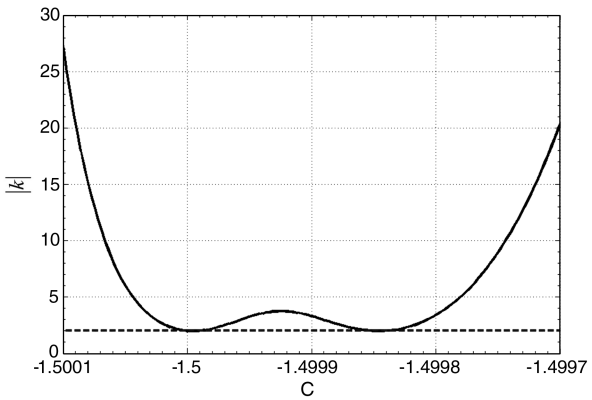

Fig. 4 Stability index versus Jacobi constant for the BUPO. The dotted line marks the stability threshold $|k| = 2$.

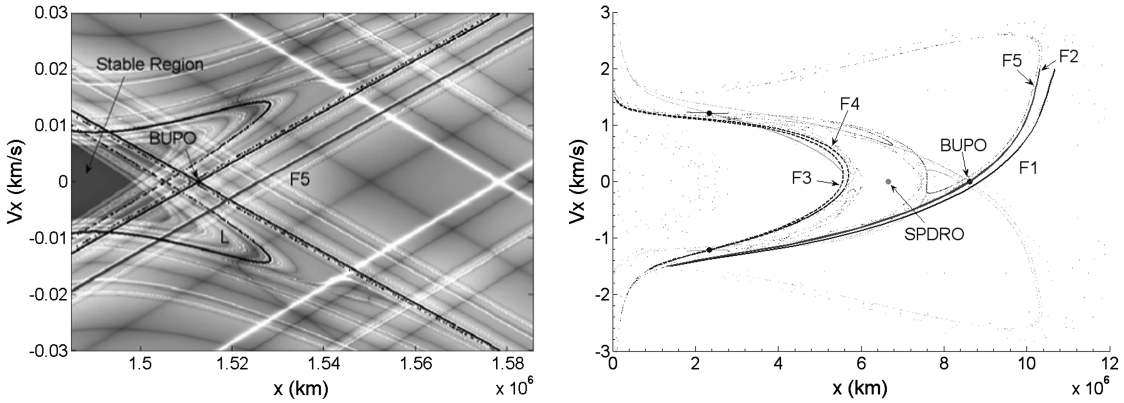

a) b)

Fig. 5 Continuations of the F1–F5 transfers at the specified energies are labeled with the stable and unstable manifolds of the BUPO at a) $C = -1.5001$ and b) $C = -1.4990$. Left image includes a fast Lyapunov indicator stability mapping with manifolds shown in black.

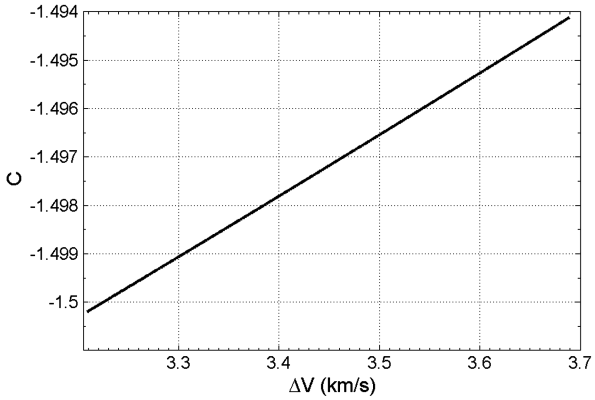

Fig. 6 ΔV versus final Jacobi constant for all single-impulse transfers.

SPDRO marking the disappearance of the stable region via the "squeeze effect" [11]. This suggests that for small ranges of energy orbits outside of the lobes may exhibit lengthy capture times. Inspection of Fig. 3a reveals that most orbits surviving at $C = -1.4997$ lie just outside due to a small index and a low probability of generating an orbit inside of a lobe. In contrast, nearly all of the survivors at $C = -1.4990$ lie inside of the lobes due to both a high index and probability of generating such an orbit.

Single-Impulse Transfers

A single-burn tangential to a circular parking orbit with an uncorrected altitude of 200 km is used. Capture lasts from when the transfer terminates on the x axis until collision or evolution into a sun-centered orbit. The simulation ends when the radius passes a certain threshold. This threshold is a multiple of the radius of Earth's Hill sphere with a multiplicative factor that increases with energy.

Figure 5a shows lobes stretching along the stable manifold originating from the first intersection of the BUPO at $C = -1.5001$. As the lobes of the stable manifold approach the BUPO they intersect the unstable manifold an infinite number of times, creating a thin region characterized by high capture periods. At all energies the stable manifolds emanating from the first crossing of the BUPO acts as a separatrix between two regions with one containing all orbits of extended capture.

Within the approximation of the CR3BP exact targeting of the stable manifold yields an infinite capture time. Realistically, this is not possible due to unmodeled forces; therefore, the area encompassed by the lobes will be investigated. A single-impulse F5 transfer traverses large regions encompassed by the lobes for a large energy range. For the lowest energies tested, $C = -1.5001$ and -1.4997, it is the only transfer that passes through any of appreciable size. Sizeable regions of extended capture are available to all families at larger energies.

The starting Jacobi constant has little variation for any position on a circular parking orbit. Thus, the variation of ΔV with final Jacobi constant for all single-impulse transfers (Fig. 6) is nearly identical for all cases.

The variation of ΔV with Vx and x position for each transfer family at a set energy is on the order of cm/s for all cases considered. Therefore, there is negligible penalty in ΔV for targeting the regions of extended capture. However, the transfer time displays significant variation. There is as much as a 63, 26, 29, 14, and 12% decrease

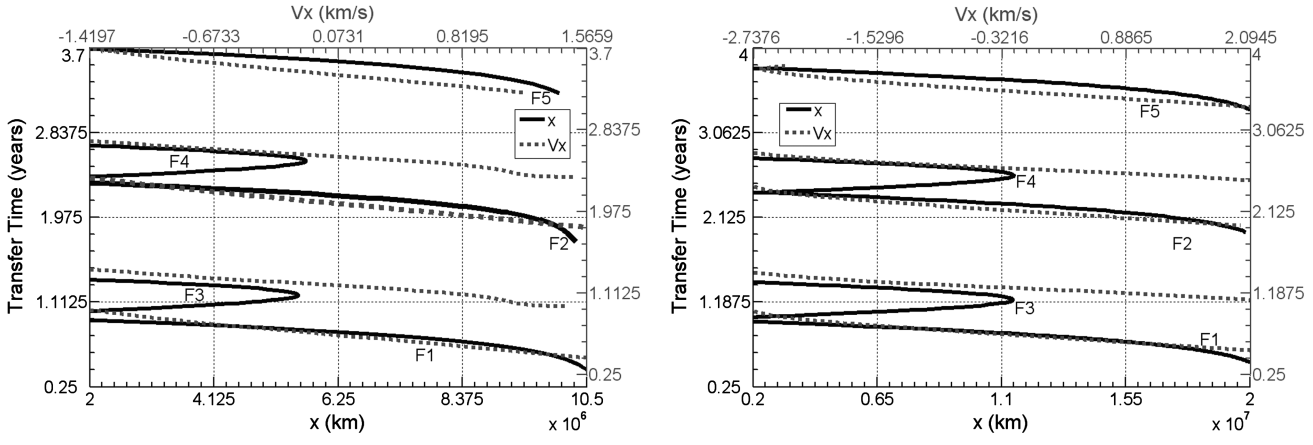

a) b)

Fig. 7 Transfer time versus x (solid line) and Vx (dotted line) for single-impulse transfers at a) $C = -1.4990$ and b) $C = -1.4960$.

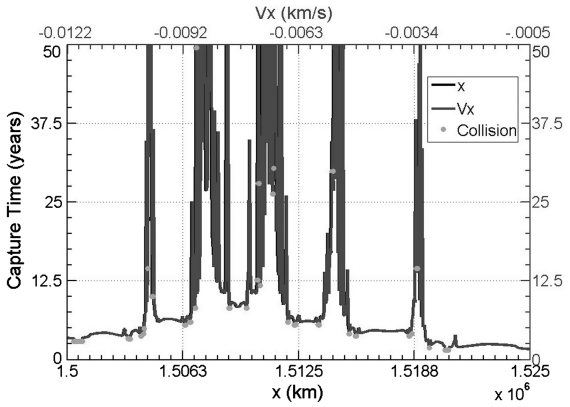

a)

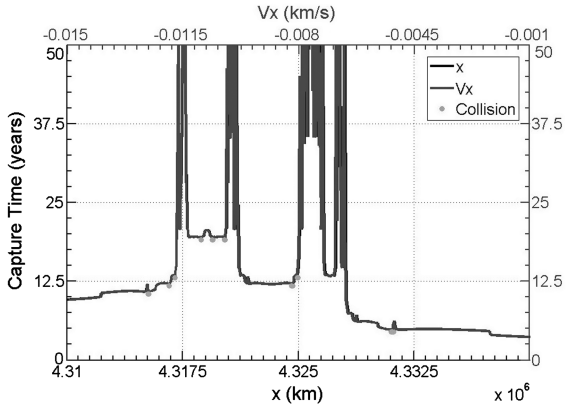

b)

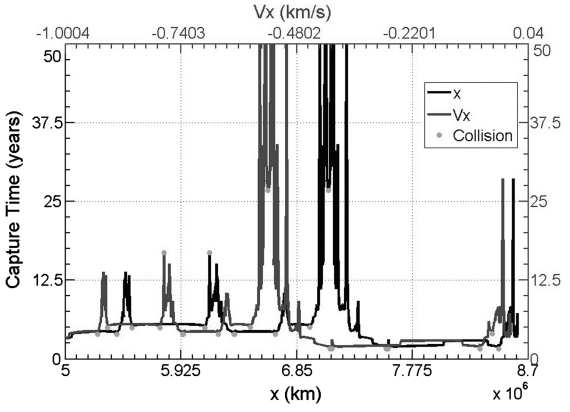

c)

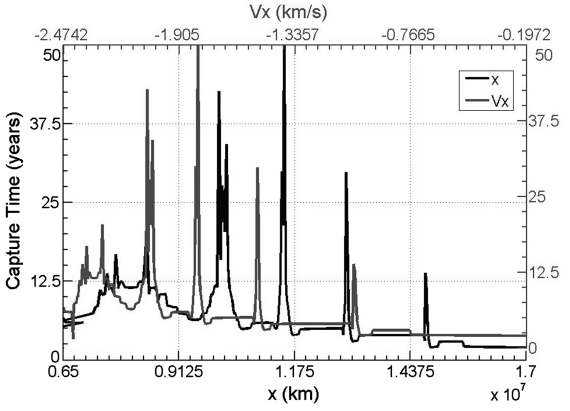

d)

Fig. 8 Variation of capture times for F5 transfer with x position at a) $C = -1.5001$, b) $C = -1.4997$, c) $C = -1.4990$, and d) $C = -1.4960$. The simulations were terminated upon collision, indicated by the dots, or after deviating a distance of 20, 20, 30, and 40 times, respectively, of the radius of Earth's Hill sphere.

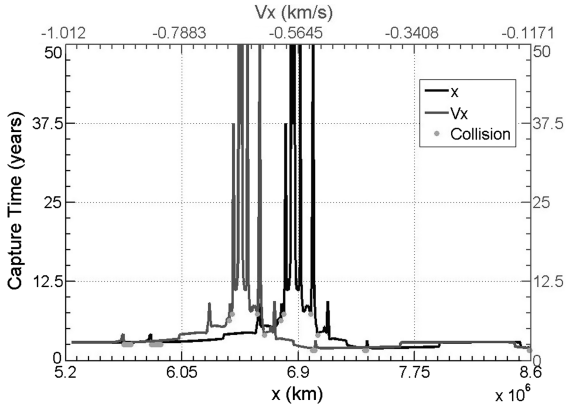

a)

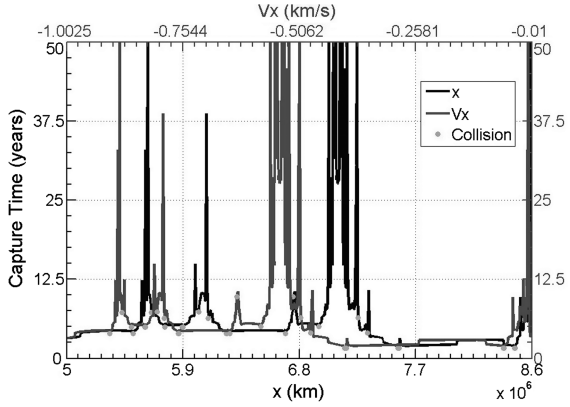

b)

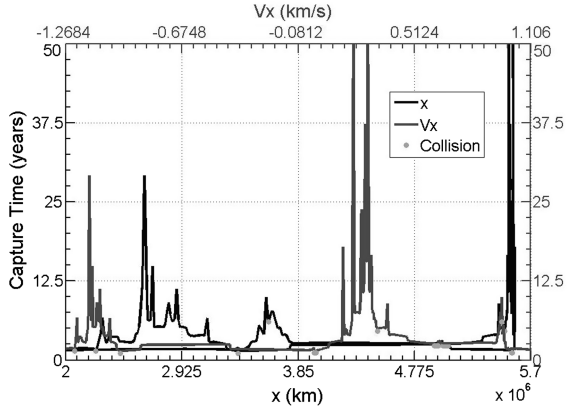

c)

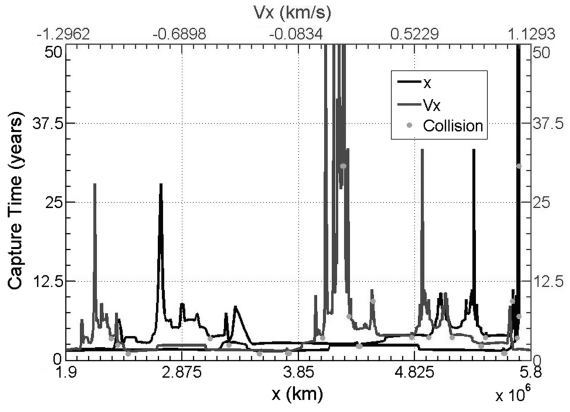

d)

Fig. 9 Variation of capture time with x position at $C = -1.4990$ for a–d) F1–F4. The simulations were terminated upon collision, indicated by dots, or after deviating a distance 30 times the radius of Earth's Hill sphere.

from the maximum time at $C = -1.4990$ for the F1–F5 curves shown in Fig. 7a. In general, the transfer time decreases with increasing Vx.

At $C = -1.5001$ the minimum capture times for single-impulse F5 transfers to a lobe are higher, by at least a few years, than in surrounding regions, see Fig. 8. The largest lobe traversed by the F5 transfer at $C = -1.5001$ extends from 1.504 to 1.515×10^6 km. The time decreases before reaching the vicinity of the stable manifold at approximately 1.519×10^6 km. Although capture is longer within the lobes, it can vary significantly. Under the idealization of the CR3BP, the shortest capture time within this lobe is about 6 years while the longest lasts in excess of 300 years. Sensitive to perturbations, exceptional orbits lie within small regions of phase space. Realistically, a spacecraft will evolve from an exceptional orbit into one possessing a lesser capture time. Large regions of extended capture, from 10 to 20 years, exist for a wide range of energies surrounding exceptional orbits.

The manifolds as well as the width of the lobes intersecting a single-impulse F5 transfer change significantly with energy. The approximate widths of the largest lobe intersected by the F5 transfer at $C = -1.5001$ and -1.4997 are 11,000 and 4000 km, respectively. However, in both cases, a target range of less than 5 m/s in Vx is required. Under some circumstances nature compensates with a low stability index. For instance, at $C = -1.4997$ the stability index is approximately 20 facilitating capture times of approximately 10 years outside of the lobes. Thus, a transfer with a minimum capture time of slightly below 10 years is possible with target dimensions in radial position and velocity of 18,725 km and 9 m/s. respectively.

At $C = -1.4990$ large lengths of the transfer, on the order of millions of kilometers, are contained within the homoclinic tangle as its width increases with energy. This is accompanied by enlarged target ranges for Vx of over 100 m/s for the largest capture times. These characteristics also exist for $C = -1.4960$, where inserting within ranges 0.5×10^6 km. and 40 m/s in radial position and velocity yields a capture time of at least 12.5 years for one target region. For both $C = -1.4990$ and -1.4960, capture times above 10 years are contained exclusively within the lobes.

All transfer families intersect sizable regions of the homoclinic tangle at larger energies. Figure 9 displays capture times for F1–F4 transfers at $C = -1.4990$. A comparison reveals that the F5 transfer possesses larger regions of persistent capture orbits as a result of the larger lengths of the F5 transfer crossing the lobes.

Collision orbits, indicated by the dots in Figs. 8 and 9, are concentrated in small pockets of space. The probability of collision drops with energy as collision sets become thinner. This conclusion is verified by the statistics given in the caption of Fig. 3. A collision at $C = -1.4997$ is 55% more likely than at $C = -1.4990$. Further simulations show that a collision at $C = -1.4999$ is 53 and 137% more likely than at $C = -1.4997$ and -1.4990.

Time-dependent perturbations due to the moon are important at the lowest energies, where orbits within the stability zone repeatedly cross its orbit. However, another study has concluded that solar radiation pressure and the moon's gravitational perturbation do not significantly affect QPDROs ranging from $1–2 \times 10^6$ km over a period of 5 years [12]. The spacecraft could have a close approach to the moon following its release from the region. Both the probability and outcome of such an event requires a more sophisticated model. Likely, it is more of a risk at lower energies.

Figure 10 shows examples of persistent capture orbits at a variety of energy levels. Science objectives may be achievable during the transfer as large segments lie within bounds defined by the amplitude of captured orbits.

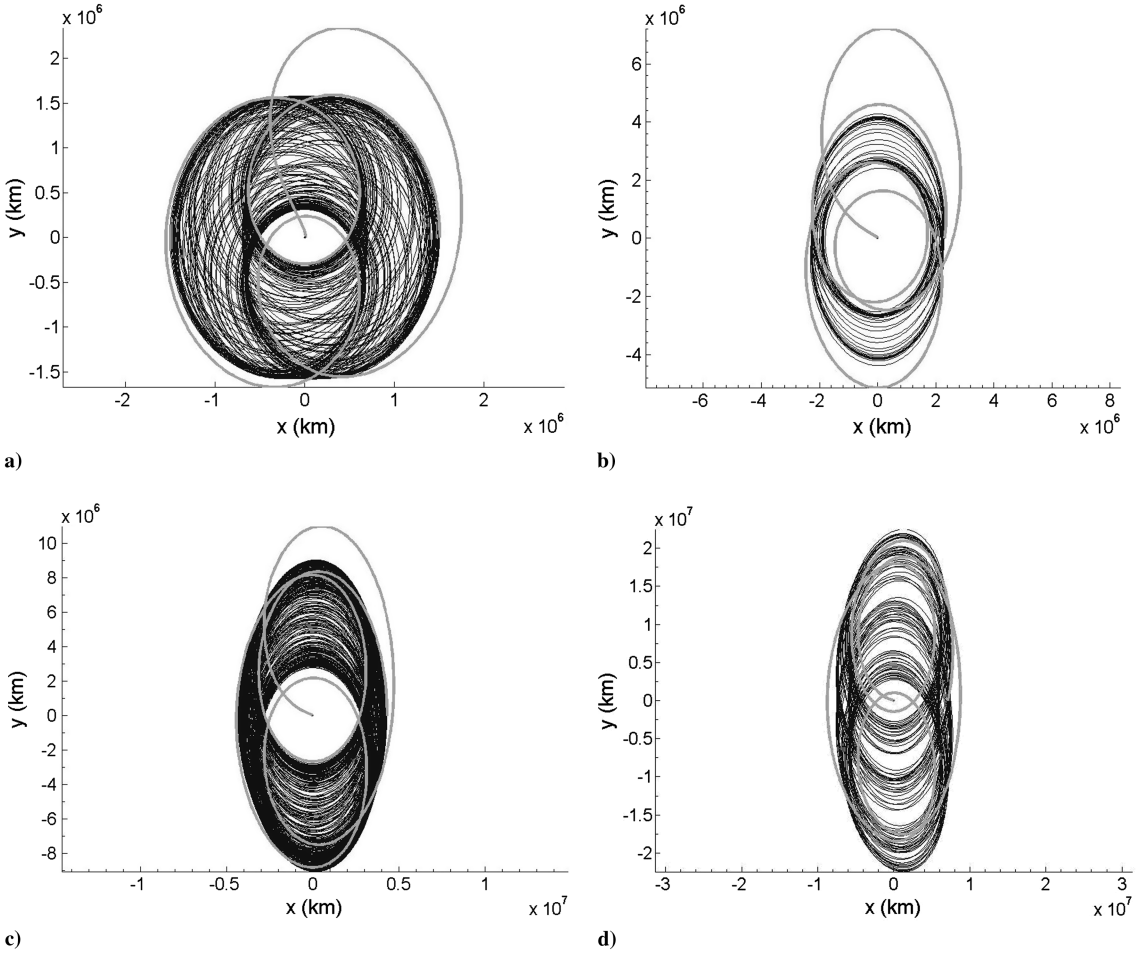

Fig. 10 Extended capture orbits at a) $C = -1.5001$, b) $C = -1.4999$, c) $C = -1.4997$, and d) $C = -1.4990$ via an F5 transfer.

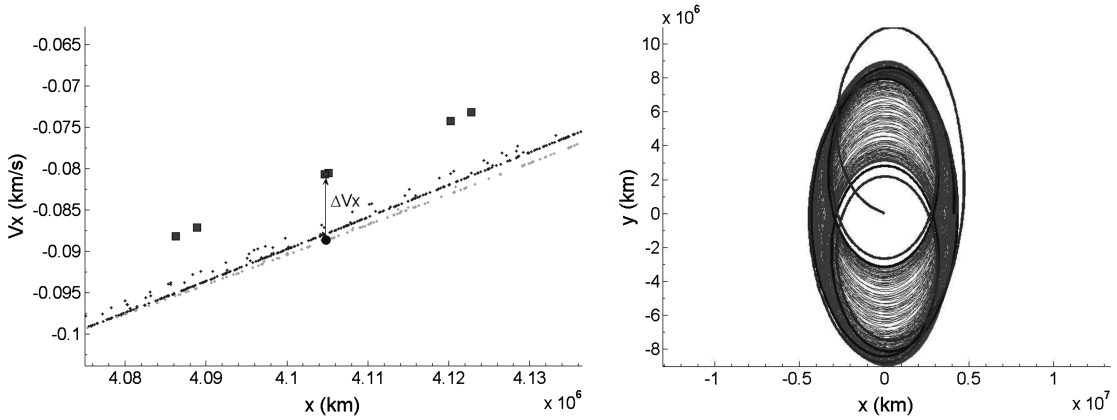

Fig. 11 At $C = -1.4997$, a) close-up of the final maneuver point with the mapping of the coast and final orbit indicated by circles and squares (mapping of the stable and unstable manifolds of the BUPO are shown in light and dark shades) and b) transfer, coast, and final orbits in physical space.

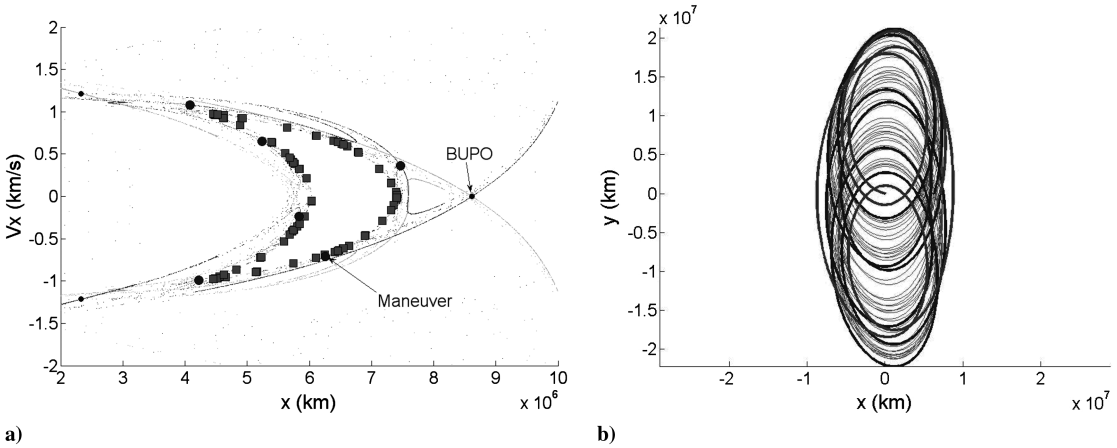

Fig. 12 At $C = -1.4990$, a) mappings of the stable and unstable manifolds of the BUPO (coast and final orbit are indicated by circles and squares) and b) transfer, coast, and final orbits in physical space.

Stabilization Maneuver

The variation of ΔV with target V_x for the F5 transfer family is within a few cm/s. Given practical constraints of orbit determination and unmodeled forces small corrective maneuvers would be necessary. More important, there is negligible penalty for inserting the spacecraft directly into an orbit possessing a lengthy capture period. This allows for incremental stabilization via a series of small maneuvers or a low-thrust propulsion system. Here, a study of the requirements of a single-impulse stabilization maneuver is made. This could be advantageous to the two-burn method of [1], in which the spacecraft would be lost in the event of an engine failure.

Figure 11 shows the mapping of an F5 transfer to an orbit of extended capture and the subsequent stabilization at $C = -1.4997$. ΔV depends on the position of the spacecraft and thickness of the homoclinic tangle. In this case, a maneuver of approximately 8 m/s is chosen to occur after a 2.6-year coasting phase. The time of the final burn was arbitrarily chosen to coincide with the third crossing of the positive x axis.

Similarly, Fig. 12 shows a stabilization maneuver of 18.7 m/s, 5.8 years after a single-impulse F5 transfer at $C = -1.4990$. In this case, the spacecraft is positioned favorably at the sixth crossing of the x axis.

These values can be compared to the ΔV required for the second impulsive transfer to the SPDRO for transfers terminating perpendicular to the x axis [1]. At the energies tested, a stabilizing maneuver translates to a ΔV savings of 82 and 85% over transfers to the SPDRO. Thus, if a QPDRO is acceptable considerable fuel savings can be realized. After the initial stabilizing burn, a series of maneuvers can be performed to reduce the amplitude of the QPDRO or to compensate for unmodeled forces. Application of optimal control theory would be worthwhile for large modifications of the QPDRO amplitude.

Conclusions

Transport rates can be completely described by the dynamical evolution of the lobes. The mathematical formalism available to describe their evolution may advance these concepts. The effects of fourth-body perturbations and other unmodeled forces remain open to investigation. The consolidation of techniques from optimal control theory and dynamics systems theory may be a fruitful concept for the design of similar transfers. Preliminary results indicate that the application of small thrust accelerations can dramatically extend the target region and period of capture. Orbits out of the ecliptic plane can avoid interference by the local zodiacal cloud and may possess larger capture times.

References

[1] Scott, C., and Spencer, D., "Calculating Transfer Families to Periodic Distant Retrograde Orbits Using Differential Correction," *Journal of Guidance, Control, and Dynamics*, Vol. 33, No. 4, 2010, pp. 1592–1605.
doi:10.2514/1.47791

[2] Alvarez-Candal, A., and Roig, F., "The Role of the Resonant 'Stickiness' in the Dynamical Evolution of Jupiter Family Comets," *IAU Symposium and Colloquium Proceedings Series*, 2004, pp. 205–208.
doi:10.1017/S174392130400866X.

[3] Hénon, M., "Numerical Exploration of the Restricted Problem. VI. Hill's Case: Non-Periodic Orbits," *Astronomy and Astrophysics*, Vol. 9, 1970, pp. 24–36.

[4] Dunham, D., "Astrodynamics-Natural Trajectories," *Space for Peace and Progress, 41st International Astronautical Congress*, Dresden, Germany, Oct. 1990.

[5] Szebehely, V., *Theory of Orbits: The Restricted Problem of Three Bodies*, Academic Press, New York, 1967, pp. 16–18.

[6] Ocampo, C., and Rosborough, G., "Transfer Trajectories for Distant Retrograde Orbiters of the Earth," *Spaceflight Mechanics 1993*, Advances in the Astronautical Sciences, Vol. 82, Pt. 2, Univelt, San Diego, CA, 1993, pp. 1177–1200.

[7] Astakhov, S., Burbanks, A., Wiggins, S., and Farrely, D., "Chaos-Assisted Capture of Irregular Moons," *Nature*, Vol. 423, 2003, pp. 264–267.
doi:10.1038/nature01622

[8] Astakhov, S., Burbanks, A., Wiggins, S., and Farrely, D., "Dynamics of Capture in the Restricted Three-Body Problem," *Order and Chaos in Stellar and Planetary Systems*, edited by G. G. Bird, K. V. Kholshevnikov, A. A. Millari, I. I. Nikiforov, and V. V. Orlov, Vol. 316, ASP Conference Series, Astronomical Society of the Pacific, San Francisco, 2004, pp. 80–85.

[9] Astakhov, S., and Farrely, D., "Capture and Escape in the Elliptic Restricted Three-Body Problem," *Monthly Notices of the Royal Astronomical Society*, Vol. 354, 2004, pp. 971–979.
doi:10.1111/j.1365-2966.2004.08280.x

[10] Wiggins, S., *Introduction to Applied Nonlinear Dynamical Systems and Chaos*, Springer–Verlag, 2nd edition, New York, 2003, pp. 612–631.

[11] Van Der Weele, J. P., Capel, H. W., Valkering, T. P., and Post, T., "The Squeeze Effect in Non-Integrable Hamiltonian Systems," *Physica A: Statistical Mechanics and Its Applications (Amsterdam)*, Vol. 147A, 1988, pp. 499–532.
doi:10.1016/0378-4371(88)90167-7

[12] Gurfil, P., and Kasdin, N., "Practical Deep-Space Geocentric and Out-of-Ecliptic Orbits in the Sun-Earth Restricted Three-Body Problem," *Proceedings of SPIE: The International Society for Optical Engineering*, Vol. 4854, 2003.
doi:10.1117/12.459820.